Electronic Supplementary Material (ESI) for CrystEngComm.
This journal is © The Royal Society of Chemistry 2024

ESI for:

An Unusual Ionic Cocrystal of Ponatinib Hydrochloride: Characterization by Single-Crystal X-ray Diffraction and Ultra-High Field NMR Spectroscopy

Alexander J. Stirk,[1,¥] Sean T. Holmes,[2,3,¥] Fabio E. S. Souza,[1] Ivan Hung,[3] Zhehong Gan,[3] James F. Britten,[4] Allan W. Rey,[1] and Robert W. Schurko,[2,3*]

[1] Apotex Pharmachem Inc., Brantford, ON, Canada N3T 6B8
[2] Department of Chemistry & Biochemistry, Florida State University, Tallahassee, FL 32306
[3] National High Magnetic Field Laboratory, Tallahassee, FL 32310
[4] MAX Diffraction Facility, McMaster University, Hamilton, ON, Canada

¥ - Denotes joint first authorship (these authors have contributed equally)
* - Denotes corresponding author

Table S1. Summary of experimental parameters for the acquisition of $^{1}H \rightarrow ^{13}C\{^{1}H\}$ ramped-amplitude CP/MAS spectra.

Pulse sequence	CP/MAS
Field / T	18.8
$\nu_0(^{1}H)$ / MHz	800.12
$\nu_0(^{13}C)$ / MHz	201.19
Time domain size	12288
Dwell time / ms	2.5
Acquisition time / ms	30.72
Spectral width / kHz	200
Number of scans	1024
Recycle delay / s	30
Spinning rate / kHz	18
^{1}H Hartmann-Hahn matching field / kHz	75
Contact time / ms	2.0
^{1}H $\pi/2$ pulse width / μs	2.5
SPINAL-64 ^{1}H decoupling field / kHz	75
Total experiment time / h	8.5

Table S2. Summary of experimental parameters for the acquisition of ^{1}H 1D and 2D BABA SQ–DQ spectra.

Pulse sequence	Hahn echo	BABA SQ–DQ
Field / T	18.8	18.8
$\nu_0(^{1}H)$ / MHz	800.12	800.12
Time domain size	2048	1024 (F2); 48 (F1)
Dwell time / ms	6.667	5.00
Acquisition time / ms	13.65	5.12 (F2); 0.48 (F1)
Spectral width / kHz	75	100 (F2); 50 (F1)
Number of scans	8	16
Recycle delay / s	6.5	6.5
Spinning rate / kHz	50	50
^{1}H $\pi/2$ pulse width / μs	2.5	2.5
Rotor periods in BABA recoupling	n/a	1
Total experiment time / min	0.87	83.2

Table S3. Summary of experimental parameters for the acquisition of ^{35}Cl spectra.

Pulse sequence	Hahn echo	Hahn echo	Hahn echo	Hahn echo
Field / T	9.4	18.8	35.2	35.2
$\nu_0(^{35}Cl)$ / MHz	39.22	78.39	146.98	146.98
$\nu_0(^{1}H)$ / MHz	400.24	800.12	1500.21	1500.21
ν_{rot} / kHz	0	0	0	16
Time domain size	512	1024	1024	4096
Dwell time / μs	2.0	1.667	5.0	2.5
Acquisition time / ms	1.02	1.71	5.12	10.24
Spectral width / kHz	250	300	100	200
Number of scans	102400	153600	16382	8192
Recycle delay / s	1.0	0.5	0.2	0.2
^{35}Cl π/2 CT selective pulse width / μs	3.75	1.67	5.0	5.0
^{1}H decoupling field / kHz	35	40	0	0
Total experiment time / h	28	21	0.9	0.5

Table S4. Summary of experimental parameters for the acquisition of the ^{35}Cl→^{1}H D-RINEPT spectrum.

Pulse sequence	D-RINEPT
Field / T	18.8
$\nu_0(^{1}H)$ / MHz	800.12
Time domain size	1024 (F2); 128 (F1)
Dwell time / ms	2.50
Acquisition time / ms	2.56 (F2); 0.64 (F1)
Spectral width / kHz	200 (F2); 100 (F1)
Number of scans	512
Recycle delay / s	0.5
Spinning rate / kHz	50
^{35}Cl π/2 CT pulse width / μs	5.0
Rotor periods of $SR4_1^2$ recoupling	5
WURST pulse width / μs	38 (followed by delay of 2)
WURST pulse rf / kHz	30 (max.)
WURST pulse offset / kHz	300
Total experiment time / min	18

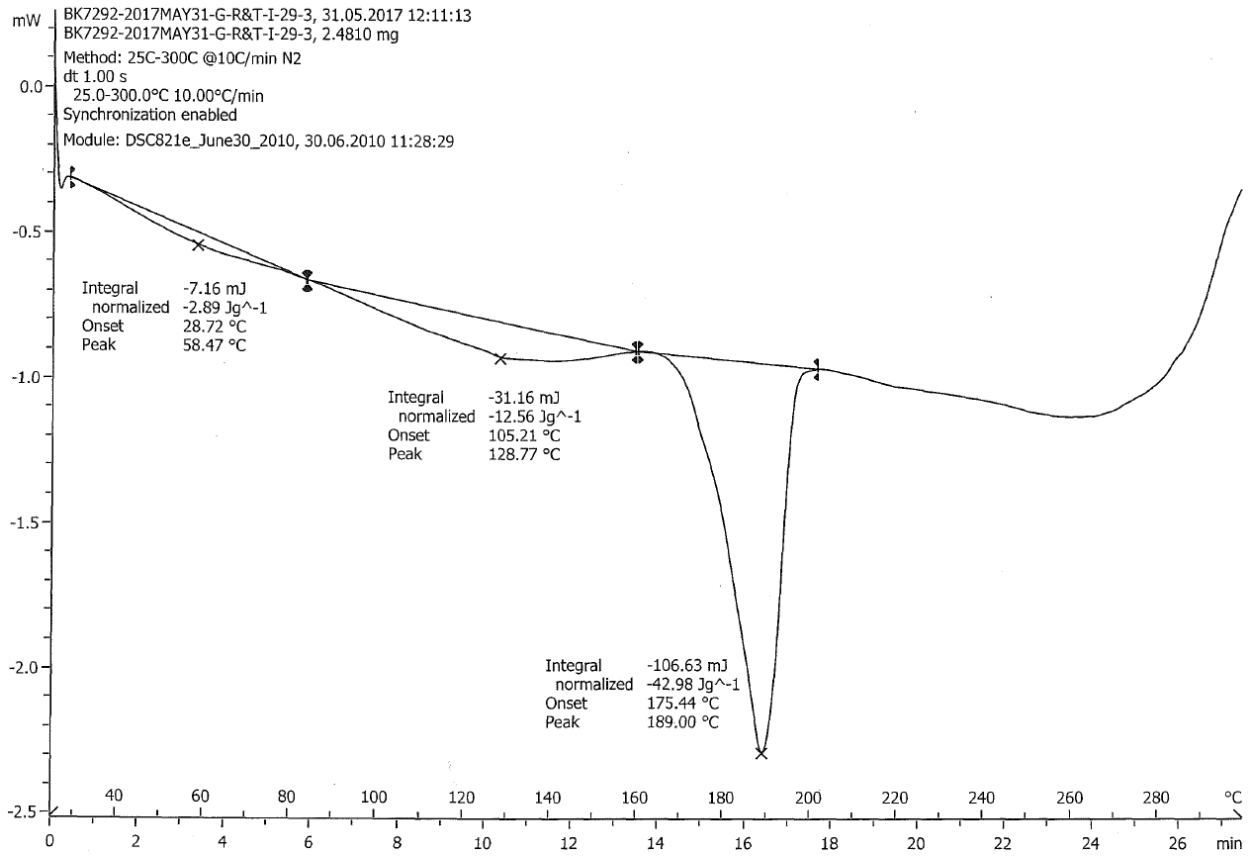

Figure S1. Differential scanning calorimetry (DSC) curve for **pon·HCl**.

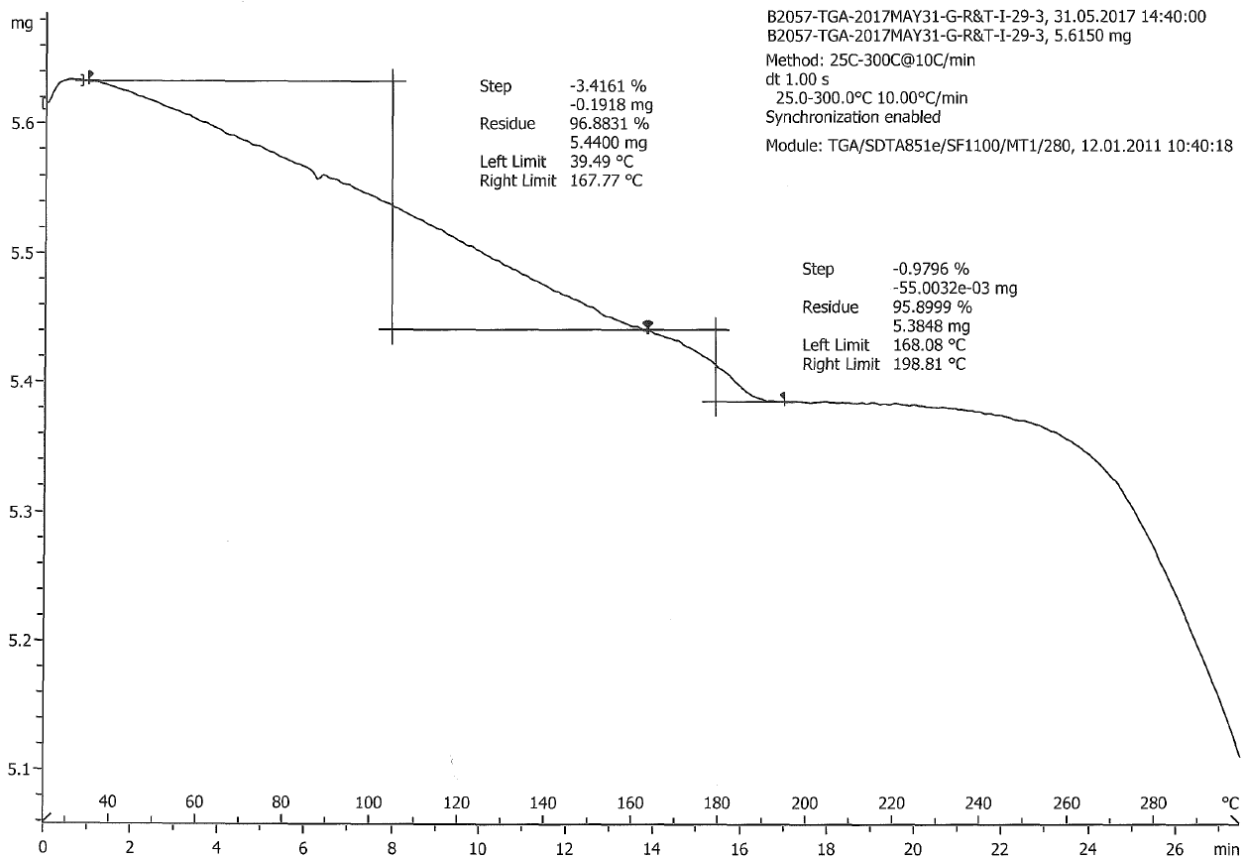

Figure S2. Thermogravimetric analysis (TGA) thermogram of **pon·HCl**.

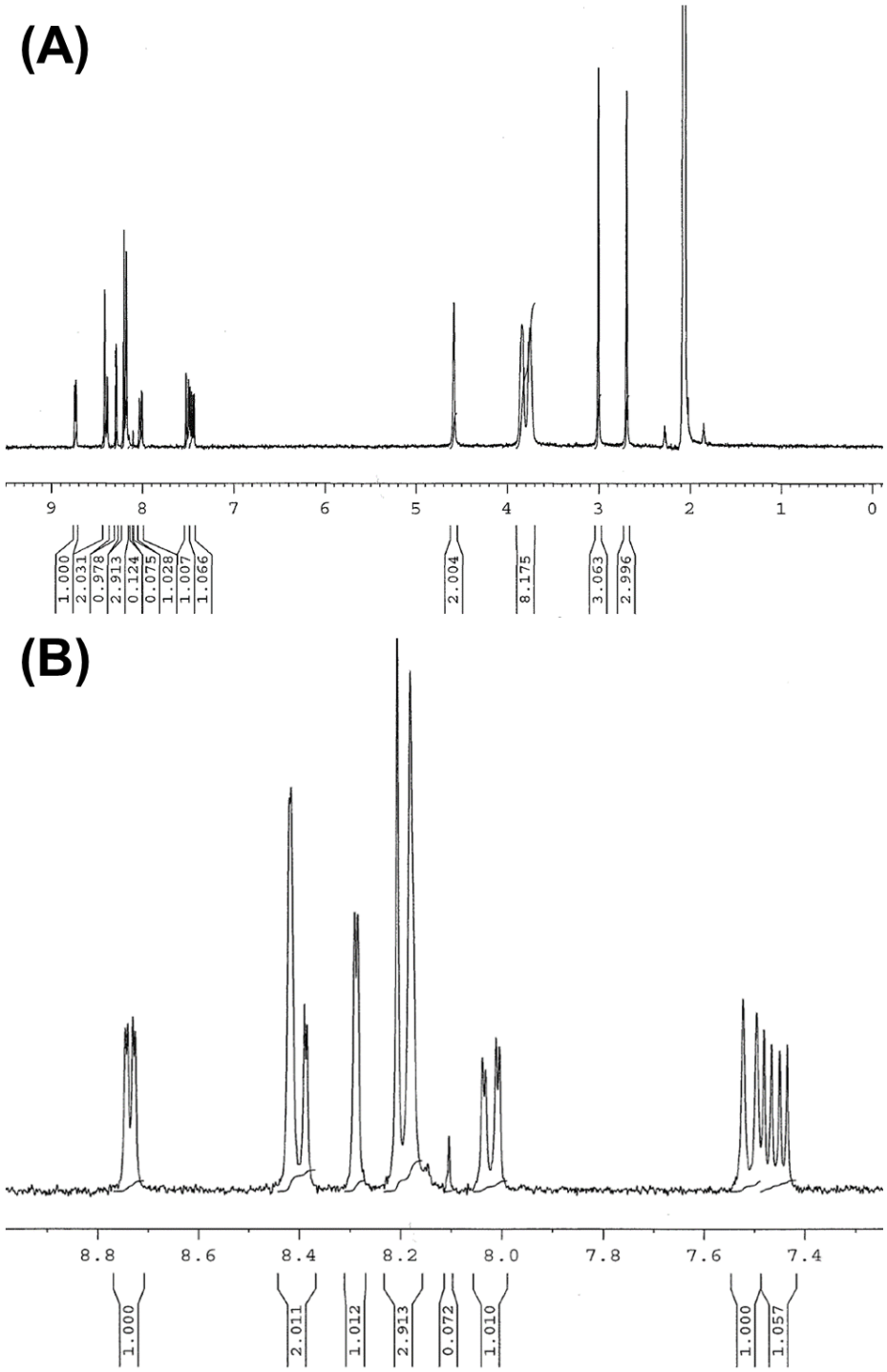

Figure S3. (A) Solution-state ^{1}H NMR spectrum of **pon·HCl** in acetic acid-d_3. (B) Detail from the solution-state ^{1}H NMR spectrum of **pon·HCl** in acetic acid-d_3.

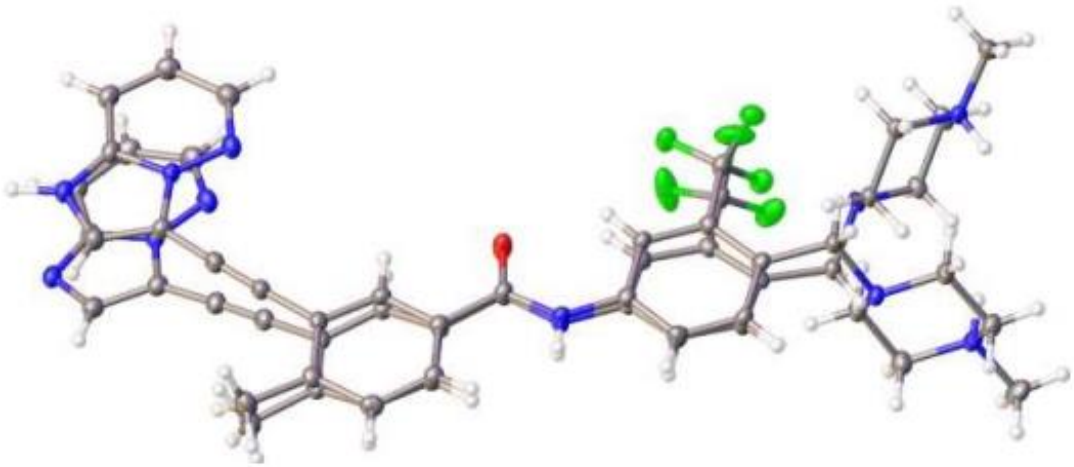

Figure S4. Molecular overlay of the ponatinib molecules A and B in the asymmetric unit.

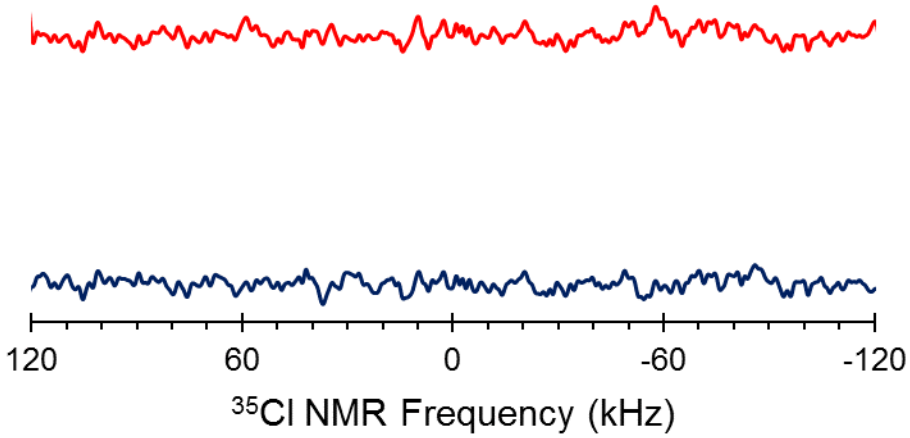

Figure S5. $^{35}Cl\{^{1}H\}$ spectra of **pon·HCl** acquired using a Bloch decay sequence, with relaxation delays of 1.0 s (blue) and 8.0 s (red). Sharp peaks arising from a potential impurity phase are not evident in either spectrum. These spectra were used to detect any potential sources of chloride ions that may be present in the bulk **pon·HCl** material.

Supplement S1: Supporting Characterization Techniques

Powder X-ray Diffraction. PXRD diffractograms were recorded on a Bruker D8 DISCOVER powder X-ray diffractometer. The sample holder was oscillated along X and Y axes during the measurement. The generator was a Micro-focus X-ray source (IMSTube: Cu tube, 1.54184 Å) with a voltage of 50 kV and current of 1.00 mA, using a divergence slit of 0.3 mm and collimator of 0.3 mm. For each sample, one frame was collected (2θ: 20.00°, Omega: 5.00°) using a still scan with a Pilatus 3R-100 kA detector over 300 s at the distance of 154.72 mm from the sample. Raw data were evaluated using the program EVA.

Thermal Analysis. Thermogravimetric analysis (TGA) and differential scanning calorimetry (DSC) data were collected using a Mettler Toledo TGA/SDTA851e Thermogravimetric Analyzer and Mettler Toledo DSC821e Differential Scanning Calorimeter, respectively. Data were collected and processed using the STARe software package. Data collection covered a temperature range of 25 – 300 °C with a heating rate of 10 °C min^{-1}, and a nitrogen gas purge rate of 85 mL min^{-1}.

Solution-state ^{1}H NMR. Solution phase ^{1}H NMR spectra were acquired using a 400 MHz Bruker Avance spectrometer. All samples were prepared in an acetic acid-d_3 solution.

Potentiometric titrations. Potentiometric titrations for chloride were conducted using a DM141-SC electrode with a solution of $AgNO_3$ (0.05 M) as a standard.

Supplement S2: Calculations of ^{1}H and ^{13}C Chemical Shifts

Calculated ^{1}H and ^{13}C isotropic magnetic shielding constants were converted to the chemical shift scale through a series of separate calculations on four materials, and comparison with experimental ^{1}H and ^{13}C chemical shifts (**Figure S6**). These material are glycine (alpha polymorph), glycine hydrochloride, L-histidine hydrochloride monohydrate, and uracil. Structural models for these materials were obtained from single-crystal X-ray diffraction studies, as deposited in the Cambridge Structural Database with CSD code of GLYCIN80, GLYHCL, HISTCM01, and URACIL. Correlations between calculated isotropic magnetic shielding constants and experimental chemical shifts yielded the following expressions from least-squares linear regression analysis:

$$\sigma_{\mathrm{iso}}\left(^{13}\mathrm{C}\right) = -1.0564 \cdot \delta_{\mathrm{iso}}\left(^{13}\mathrm{C}\right) + 186.93 \text{ ppm} \qquad \text{Eq. S1}$$

$$\sigma_{\mathrm{iso}}\left(^{1}\mathrm{H}\right) = -1.0976 \cdot \delta_{\mathrm{iso}}(\mathrm{H}) + 31.63 \text{ ppm} \qquad \text{Eq. S2}$$

These equations were used to convert the calculated ^{1}H and ^{13}C isotropic magnetic shielding constants for **pon·HCl** to their respective chemical shift scales. Similarly, the calculated ^{35}Cl isotropic magnetic shielding constant of **pon·HCl** was converted to the chemical shift by setting the calculated shielding constant for L-histidine hydrochloride monohydrate to 34.5 ppm from aqueous NaCl.

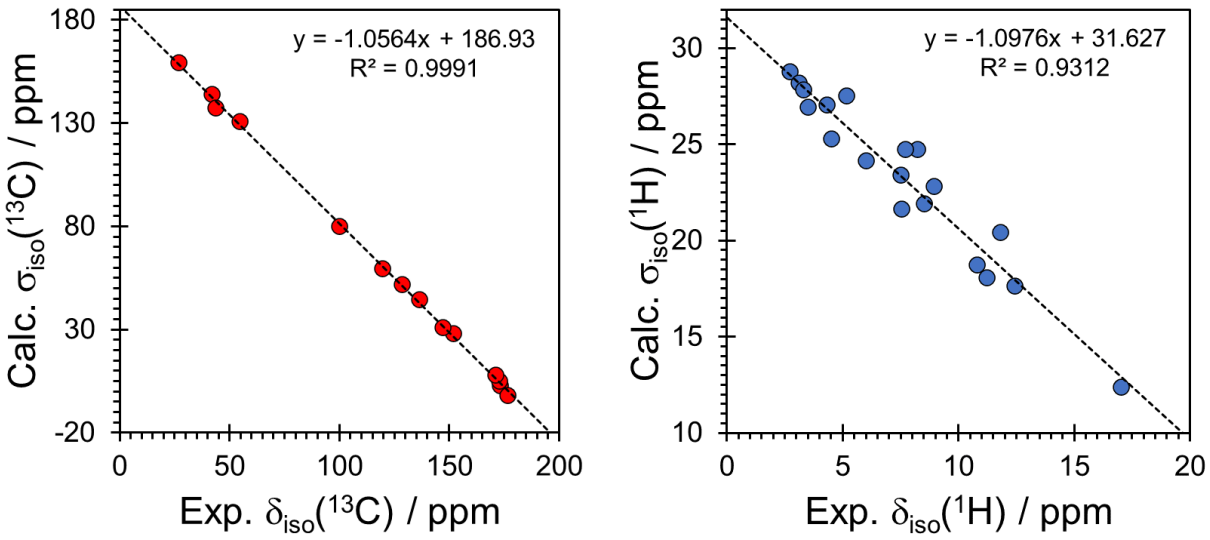

Figure S6. Correlations between calculated isotropic magnetic shielding and experimental chemical shifts for L-histidine HCl·H_2O. Results are shown for ^{1}H (left) and ^{13}C (right). Calculations were performed at the PBE0 level, as describe in the main text.

Table S5. Summary of calculated ^{13}C isotropic chemical shifts for **pon·HCl**.

Carbon Label	Moiety	Calc. Shift (ppm)	Carbon Label	Moiety	Calc. Shift (ppm)
	Molecule A			**Molecule B**	
1a	aromatic, protonated	151.1	1b	aromatic, protonated	144.0
2a	aromatic, protonated	126.8	2b	aromatic, protonated	122.1
3a	aromatic, protonated	126.0	3b	aromatic, protonated	129.1
4a	aromatic, non-protonated	133.5	4b	aromatic, protonated	138.2
5a	aromatic, protonated	130.7	5b	aromatic, protonated	140.3
6a	aromatic, protonated	115.8	6b	aromatic, protonated	114.3
7a	acetylenic	84.5	7b	acetylenic	91.4
8a	acetylenic	103.5	8b	acetylenic	104.1
9a	aromatic, protonated	119.1	9b	aromatic, protonated	124.5
10a	aromatic, protonated	133.9	10b	aromatic, protonated	132.1
11a	aromatic, protonated	129.2	11b	aromatic, protonated	128.2
12a	aromatic, protonated	130.6	12b	aromatic, protonated	126.7
13a	aromatic, protonated	134.5	13b	aromatic, protonated	129.0
14a	aromatic, protonated	146.0	14b	aromatic, protonated	147.4
15a	R-CH_3	22.8	15b	R-CH_3	26.9
16a	amide	161.4	16b	amide	160.4
17a	aromatic, protonated	138.1	17b	aromatic, protonated	137.5
18a	aromatic, protonated	123.4	18b	aromatic, protonated	121.4
19a	aromatic, protonated	133.2	19b	aromatic, protonated	131.3
20a	aromatic, protonated	131.6	20b	aromatic, protonated	134.2
21a	aromatic, protonated	128.6	21b	aromatic, protonated	130.4
22a	aromatic, protonated	117.5	22b	aromatic, protonated	117.6
23a	CF_3	131.5	23b	CF_3	131.3
24a	CH_2	56.6	24b	CH_2	57.1
25a	CH_2	51.5	25b	CH_2	51.0
26a	CH_2	52.8	26b	CH_2	54.9
27a	CH_2	51.0	27b	CH_2	51.0
28a	CH_2	47.8	28b	CH_2	48.2
29a	N-CH_3	42.2	29b	N-CH_3	42.1

Table S6. Summary of calculated ^{1}H isotropic chemical shifts for **pon·HCl**.

Hydrogen Label	Moiety	Calc. Shift (ppm)	Hydrogen Label	Moiety	Calc. Shift (ppm)	Hydrogen Label	Calc. Shift (ppm)
	Molecule A			**Molecule B**		**Waters**	
H1A	imidazopyridazine	18.2				H1C,D	4.1
H1AA	aromatic	10.5	H1B	aromatic	8.5	H2C,D	4.0
H2A	aromatic	8.9	H2B	aromatic	8.8	H3C,D	5.1
H3A	aromatic	7.7	H3B	aromatic	8.7		
H4A	amide	7.6	H4B	amide	6.0		
H5A	aromatic	10.6	H5B	aromatic	9.6		
H6A	amine	8.1	H6B	amine	6.2		
H10A	aromatic	7.3	H10B	aromatic	7.8		
H12A	aromatic	9.2	H12B	aromatic	8.1		
H13A	aromatic	8.1	H13B	aromatic	7.4		
H15A,B,C	R-CH_3	-0.4	H15D,E,F	R-CH_3	3.4		
H18A	aromatic	8.3	H18B	aromatic	7.5		
H19A	aromatic	7.4	H19B	aromatic	6.9		
H22A	aromatic	8.5	H22B	aromatic	8.2		
H24A,B	CH_2	2.9	H24C,D	CH_2	2.0		
H25A,B	CH_2	3.3	H25C,D	CH_2	3.6		
H26A,B	CH_2	3.9	H26C,D	CH_2	4.1		
H27A,B	CH_2	5.0	H27C,D	CH_2	4.5		
H28A,B	CH_2	3.2	H28C,D	CH_2	3.1		
H29A,B,C	N-CH_3	3.7	H29D,E,F	N-CH_3	4.2		

Supplement S3:

Previous work has demonstrated that those hydrogen bonds with H···Cl^- distances of 2.2 Å or less, which we refer to as *short contacts*, most strongly influence the signs, magnitudes, and orientations of the principal components of ^{35}Cl EFG tensors; similarly, hydrogen bonds up to 2.6 Å[1] may impact the EFGs, but their effects are typically less significant when short contacts are also present.[2-5] For a chloride ion featuring a single short contact, DFT calculations typically predict that the sign of C_Q is negative and the largest principal component, V_{33}, resides close to the hydrogen bonding axis (*i.e.*, the value of the EFG is positive along this axis, since $Q(^{35}\text{Cl}) = -8.112$ fm^2).[6] Chloride ions featuring two short contacts oriented with an angle near ∠(H-Cl-H) = 180° behave analogously to one-contact systems.[5] Both of these spatial arrangements tend to have large associated values of C_Q and values of η_Q near zero (*i.e.*, axial or near-axial symmetry). In contrast, chloride ions featuring two short contacts in which ∠(H-Cl-H) ≠ 180° are predicted to have positive values of C_Q, with V_{33} oriented approximately perpendicular to the plane formed by the short contacts. These sites typically have lower magnitudes of C_Q, as well as values of η_Q that deviate from axial symmetry. Furthermore, chloride sites featuring hydrogen bonds involving water molecules have recently been investigated.[7] When systems lack short contacts, the EFGs are influenced by many weak interactions, and the relationships between EFGs and structure are less obvious; these sites must be considered on a case-by-case basis.

References

(1) Steiner, T. Hydrogen-bond distances to halide ions in organic and organometallic crystal structures: up-to-date database study. *Acta Crystallogr., Sect. B* **1998**, *54*, 456-463.
(2) Hamaed, H.; Pawlowski, J. M.; Cooper, B. F. T.; Fu, R.; Eichhorn, S. H.; Schurko, R. W. Application of solid-state ^{35}Cl NMR to the structural characterization of hydrochloride pharmaceuticals and their polymorphs. *J. Am. Chem. Soc.* **2008**, *130*, 11056-11065.
(3) Hildebrand, M.; Hamaed, H.; Namespetra, A. M.; Donohue, J. M.; Fu, R.; Hung, I.; Gan, Z.; Schurko, R. W. ^{35}Cl solid-state NMR of HCl salts of active pharmaceutical ingredients: structural prediction, spectral fingerprinting and polymorph recognition. *CrystEngComm* **2014**, *16*, 7334-7356.
(4) Holmes, S. T.; Hook, J. M.; Schurko, R. W. Nutraceuticals in bulk and dosage forms: analysis by ^{35}Cl and ^{14}N solid-state NMR and DFT calculations. *Mol. Pharm.* **2022**, *19*, 440-455.
(5) Peach, A. A.; Hirsh, D. A.; Holmes, S. T.; Schurko, R. W. Mechanochemical syntheses and ^{35}Cl solid-state NMR characterization of fluoxetine HCl cocrystals. *CrystEngComm* **2018**, *20*, 2780-2792.
(6) Pyykkö, P. Year-2017 nuclear quadrupole moments. *Mol. Phys.* **2018**, *116*, 1328-1338.
(7) Holmes, S. T.; Vojvodin, C. S.; Veinberg, N.; Iacobelli, E. M.; Hirsh, D. A.; Schurko, R. W. Hydrates of active pharmaceutical ingredients: a ^{35}Cl and ^{2}H solid-state NMR and DFT study. *Solid State Nucl. Magn. Reson.* **2022**, *122*, 101837.